AIP | The Journal of Chemical Physics

X-ray spectroscopy studies on the surface structural characteristics and electronic properties of platinum nanoparticles

Z. Bayindir, P. N. Duchesne, S. C. Cook, M. A. MacDonald, and P. Zhang

Citation: The Journal of Chemical Physics **131**, 244716 (2009); doi: 10.1063/1.3276917
View online: http://dx.doi.org/10.1063/1.3276917
View Table of Contents: http://scitation.aip.org/content/aip/journal/jcp/131/24?ver=pdfcov
Published by the AIP Publishing

X-ray spectroscopy studies on the surface structural characteristics and electronic properties of platinum nanoparticles

Z. Bayindir,[1] P. N. Duchesne,[1,2] S. C. Cook,[1,2] M. A. MacDonald,[1,2] and P. Zhang[1,2,a)]
[1]*Institute for Research in Materials, Dalhousie University, Halifax, Nova Scotia B3H 4J3, Canada*
[2]*Department of Chemistry, Dalhousie University, Halifax, Nova Scotia B3H 4J3, Canada*

(Received 3 October 2009; accepted 3 December 2009; published online 31 December 2009)

The surface structural characteristics and electronic behavior of three platinum nanoparticle (NP) samples prepared with tertiary amine (Pt-TA), primary amine (Pt-PA), and thiol (Pt-SR) molecules were studied using Pt 4f, 5d, and S 2p x-ray photoelectron spectroscopy (XPS), Pt L_3-edge x-ray absorption spectroscopy (XAS), and theoretical projected local density of states (l-DOS) calculations. Transmission electron microscopy and XPS composition analysis indicated that the three NPs were all very small (1–2 nm), the NP size decreasing in the order of Pt-TA > Pt-PA ~ Pt-SR. All the three samples showed a positive Pt 4f binding energy (BE) shift relative to that of the bulk, in the order of bulk < Pt-TA < Pt-PA < Pt-SR. The origin of the BE shift was elucidated by XAS and deconvolution of the Pt 4f XPS peak, indicating that the observed BE shifts were largely associated with the initial state effect (i.e., nanosize and surface structure). The surface and size effects on the electronic behavior of Pt were further studied by valence band XPS and the results were interpreted with calculated d-DOS of three Pt_{55} model clusters with varied surface structures. Finally, the implication of these results on tuning the electronic properties of Pt NPs with size, surface, and alloying effects was discussed. © *2009 American Institute of Physics*. [doi:10.1063/1.3276917]

I. INTRODUCTION

Studies on the surface property and electronic behavior of platinum nanoparticles (NPs) are of paramount importance in both fundamental studies and technological applications.[1,2] Recently, significant advances have been achieved in the preparation of molecularly capped metal NPs (i.e., NPs consisting of an inorganic core coated with organic molecules).[3,4] The molecule-capping method has shown various advantages over other preparative methods, such as low preparation cost and better control of NP structure in terms of particle size, monodispersity, and shape.[5] One unique feature of such a molecule-capping route is that the NP surfaces are capped with organic molecules. The capping molecules serve to surface functionalize as well as stabilize the NPs. Many promising applications can be foreseen in association with the molecular capping of NPs, in areas such as biodetection, drug delivery, and chiral catalysis.[4] In this context, it is very important to understand the surface capping effect on the electronic properties of the NPs in connection with the metal-molecule interaction. In addition, studies on size varied NPs are also important to elucidate the surface property as the particle size directly determines the surface area of NPs.[6]

Here, we present a study of molecularly capped Pt NPs using Pt 4f and valence band x-ray photoelectron spectroscopy (XPS), Pt L_3-edge x-ray absorption spectroscopy (XAS), and Pt projected local density of states (l-DOS) calculations. We show experimental results on effects of nanosize and surface structure on the core level and valence band XPS and illustrate the mechanism of size and surface effects on the electronic property of Pt NPs by correlating the experimental x-ray results with calculated d-DOS data. Finally, we show that by systematically tailoring the surface structure, particle size, and alloying composition, fine-tuning of the electronic properties of Pt NPs can be possibly achieved.

II. EXPERIMENTAL SECTION

Platinum NPs were prepared using a reverse micelle method originally reported by Brust *et al.*[7] The two NP samples capped with weakly interacting molecules (primary and tertiary amines) were prepared by the following procedure. In brief, 0.06 mmol hydrogen hexachloroplatinate hydrate ($H_2PtCl_6 \cdot 6H2O$) was dispersed into 30 ml of toluene in the presence of 0.18 mmol didodecyldimethylammonium bromide by sonication. Next, 0.72 mmol of amine (1-dodecylamine, DDA, or tri-n-dodecylamine) was added to the toluene suspension. Under Ar protection the toluene solution was vigorously stirred before sodium borohydride and 20 μl water was added to reduce Pt (IV) to Pt (0) to form molecularly capped NPs. The reactions were further kept running for 2 h under Ar protection. Most of the toluene was then removed by a rotary evaporator. Next, 100–200 ml ethanol was added to the reaction mixture to cause precipitation. The precipitate was collected by centrifuge and then redispersed with toluene and centrifuged again to remove the insoluble components. Finally, the purified NP samples were stored in toluene under Ar protection. The Pt NPs capped with strongly interacting dodecanethiol molecules were prepared by a capping molecule exchange reaction. First, Pt NPs

a)Author to whom correspondence should be addressed. Tel.: 001-902-4943323. FAX: 001-902-4941310. Electronic mail: peng.zhang@dal.ca.

were prepared with weakly capped molecules (DDA, Pt:DDA=1:12). Next, under Ar protection dodecanethiol (Pt:HSR=1:10) was added to the NP suspension to conduct the capping molecule exchange reaction for 1 h. The thiol-capped NPs were finally purified with the ethanol precipitation method described above. In this work, the Pt NPs prepared with primary amine (PA) are referred to as Pt-PA, the ones with tertiary amine as Pt-TA, and thiol-capped NPs as Pt-SR. These titles (Pt-PA, Pt-TA, and PT-SR) were not intended to represent the actual composition of the NPs; instead, they were used to emphasize the different binding effect of the highlighted capping molecules (PA, TA, and SR) that significantly influenced the structure and electronic properties of the NPs.

The XPS experiment was performed with a Multilab 3000 XPS system manufactured by Thermo VG Scientific. The XPS data were collected with a dual anode x-ray source using Mg Kα irradiation with the energy of 1253.6 eV. Binding energies were measured using a hemispherical energy analyzer set to 50 eV pass energy in constant analyzer energy mode. The composition analysis was conducted with the VG Avantage V.3.99 program, using the core level peaks of $Pt_{7/2}$, S_{2p}, and N_{1s}. The sampling depth was estimated to be in the range of 1–10 nm. The XPS binding energies were calibrated using the carbon (285.00 eV) 1s peak. X-ray radiation-induced damage of the light elements (e.g., carbon) in the capping molecules was possible during the XPS measurements. However, the present work was focused on the x-ray studies of the Pt core (e.g., Pt 2p, 4f, and 5d levels), which should not be influenced by the partial damage of the capping molecules. Nevertheless, if a detailed XPS analysis of the capping molecules is desired, a careful control of the x-ray dose is preferred to avoid the radiation-induced damage.

The transmission electron microscope (TEM) images of NPs are taken from a JEM 1230 TEM operated at 80 kV. The synchrotron Pt L_3-edge XAS experiments were performed at the HXMA beamline of Canadian Light Source (CLS) using a transmission mode. The Pt NPs were dispersed in toluene in a Teflon XAS cell. A simultaneous collection of the XAS data of Pt foil was performed for each measurement to ensure a reliable measurement of the E_0 shift of the NPs relative to the bulk reference. The x-ray absorption fine structure (XAFS) data were normalized using the standard procedure previously described.[8,9]

The l-DOS calculation was conducted using the FEFF8 program.[10] The Crystal Maker program was used to construct model clusters Pt_{55}, $Pt_{55}O_{24}$, $Pt_{55}S_{24}$, and bulk Pt (141 atoms), generating the atomic coordinates for the FEFF input file. Only one specific surface site (see the description in Sec. III C) of the model clusters was selected for the l-DOS calculation to illustrate the nanosize and surface effects. The calculation was conducted by completely screening the core hole using a NOHOLE card because the NOHOLE approach gives better agreement for d-DOS and L-edge absorption calculations.[10]

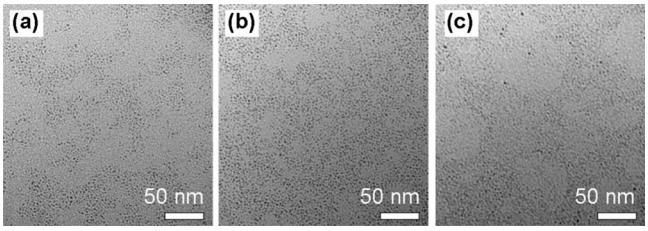

FIG. 1. Representative TEM images of Pt-TA (a), Pt-PA (b), and Pt-SR (c).

III. RESULTS AND DISCUSSION

A. Structural and composition analysis

Figure 1 shows the TEM images of three Pt NPs. The NPs are all very small, in the range of 1–2 nm in diameter. Such a size range implies about 100–300 atoms per particle, with >50% Pt atoms on the surface. To obtain more structural information of the NPs, XPS composition analysis was performed. The results are presented in Table I. For a convenient comparison of the elemental composition in each NP, the concentration of Pt atoms is set to be 100%. The molecule-to-Pt molar ratio of Pt-TA (0.59) is found to be significantly smaller than that of Pt-PA (1.3). These results suggest that the surface area of Pt-TA per volume is smaller than that of Pt-PA. In other words, the average particle size of Pt-TA is bigger than that of Pt-PA. We have recently reported the preparation of Au NPs using primary and tertiary amines under similar conditions, yielding an average size of 2.8 nm for the former and 5.1 nm for the latter.[11] Our finding that Pt-TA is bigger than Pt-PA is in agreement with the results of Au NPs. It should be noted that a TA occupies more space on the NP surface than a PA does, which should also contribute to the lower molecule-to-Pt ratio of Pt-TA. The fact that molecule-to-Pt ratio of Pt-PA and Pt-SR is identical (both are 1.3) indicates that the two NP samples have essentially the same size. Therefore, the three Pt samples represent two interesting systems: (i) size-varied NPs with similar capping molecules (amines) and (ii) same-sized NPs with varied protecting molecules (strongly interacting thiols versus weakly interacting amines).

From Table I, it is also seen that amine and bromide are both present in the two weakly bound NPs, with similar molar ratio of amine to Br (2.8 for Pt-TA and 2.6 for Pt-PA).

TABLE I. XPS composition analysis of three Pt NPs.

Sample	Pt (%)[a]	N (%)	Br (%)	Amine (%)	Amine/Br	S (%)	Molecules/Pt
Pt-TA	100	58.7	15.5	43.2	2.8	···	0.59
Pt-PA	100	131	36.9	94.1	2.6	···	1.3
Pt-SR	100	71.6	···	71.6	···	59.4	1.3

[a]The concentration of Pt is set to be 100% for each sample.

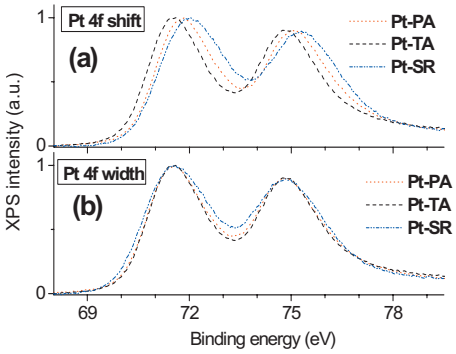

FIG. 2. A comparison of (a) the BE shift and (b) spectral shape of Pt 4f XPS of three Pt NPs.

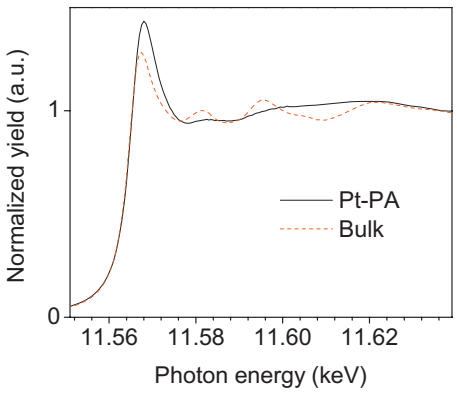

FIG. 3. Pt L_3-edge XANES of Pt-PA and the bulk.

The unusually high molecule-to-Pt ratio (>1) for Pt-PA and Pt-SR cannot be interpreted with the normal surface bonding model of NPs. It is likely due to the high surface inhomogeneity of the small NPs, that is, the presence of surface atoms with very low coordination number, to which more than one PA molecules are bonded. This hypothesis is in agreement with the finding of a low molecule-to-Pt ratio for Pt-TA (0.59), since bonding of >1 bulky TA molecules to a surface Pt atom is not favored. Interestingly, when thiols were used in the molecules-exchange reaction, the bromide capping molecules were found to be completely replaced (no Br was detected in the XPS analysis). In addition, thiols also replaced some of the PA, that is, the amine percent decreases from 94% to 72% when going from Pt-PA to Pt-SR.

B. Core-level XPS and L_3-edge XAS results

Pt 4f XPS data are presented in Fig. 2. In Fig. 2(a) the binding energy (BE) shift of the NPs are compared and in Fig. 2(b) the line width is compared by lining up the 4f peaks of Pt-PA and Pt-SR with that of Pt-TA. Pt 4f data of the NPs together with that of the bulk, i.e., peak position and line width, are also given in Table II. A couple of important observations are noted. First, all the three NPs exhibit a positive BE shift relative to the bulk in the order of Pt-TA <Pt-PA <Pt-SR. Second, there is a linewidth broadening relative to the bulk in the same order, i.e., Pt-TA <Pt-PA <Pt-SR. This broadening is accompanied with a systematic increase in the asymmetry at the higher BE side of the Pt 4f peak, similar to the results of thiol-protected Au NPs reported by Zhang and Sham.[12] Here we first focus on the discussion of the two weakly bound NPs of varied size (Pt-TA and Pt-PA). A comparison of the surface capping effect (Pt-PA versus Pt-SR) will be addressed later in this section. The observed asymmetric broadening of Pt 4f peaks for Pt-TA and Pt-PA can be attributed to both the increased inhomogeneity of Pt atoms in the NP surface and the presence of more localized unoccupied d states at the Fermi level, enhancing a many-body effect often known as Doniach–Sunjic line shape.[13] Regarding the core-level BE shift of transition metal NPs, it has been proposed that two mechanisms are responsible.[14] The first mechanism is the initial-state effect which is due to the changed electronic configuration of the metal atoms in the NCs.[15] The second one is known as final-state effect, such as the Coulomb charging effect associated with small metal clusters (note: the Coulomb charging effect refers to the presence of a core-hole that is not neutralized on the time scale of femtoseconds of the photoemission process, different from the XPS charging phenomenon of an insulator).[16] To illustrate the origin of the positive core-level BE shift discussed above, we next turn to the Pt L_3-edge x-ray absorption near edge structure (XANES) results. XANES is a complementary tool to XPS in the study of electronic properties of metal NPs and can provide helpful information to interpret the origin of XPS BE shift.[17]

TABLE II. Pt 4f data [Databased on the spectra in Fig. 2 (not deconvoluted) with an uncertainty of 0.10 eV] of three NPs and the bulk.

Sample	$4f_{7/2}$ maximum (eV)	$4f_{7/2}$ width (eV)
Pt-TA	71.45	1.67
Pt-PA	71.70	1.74
Pt-SR	71.83	1.80
bulk	71.20	1.50

Figure 3 shows the XANES of one Pt sample, Pt-PA. As a reference, the XANES of Pt foil is also shown. The sharp peak right after the edge jump for both samples observed in Fig. 3 is historically called white line.[18] The Pt L_3-edge white line probes the electronic transition from 2p to unoccupied 5d states.[18] A more intense white line corresponds to more unoccupied 5d states (d-hole) or less 5d electrons. The electronic configuration of single Pt atom is $5d^9 6s^1 6p^0$.[19] However, due to the s-p-d hybridization, a small amount of 5d electron (0.34 e^-) is transferred to s-p states when 5d band is formed in bulk Pt.[20] As a result, bulk Pt has an electronic configuration of $d^{8.66}s^{0.77}p^{0.58}$.[20] For plain Pt NPs (i.e., with no other surface species), the 5d band becomes narrower as the size decreases, leading to less s-p-d hybridization.[19] Consequently, the d electron count of Pt atoms in NPs should be greater than that of bulk, i.e., 8.66 <d<9.[9] This s-p-d band rehybridization model is also supported by our l-DOS calculation results presented later (Table IV). Returning to Fig. 3, the most striking difference between the XANES of NPs and bulk Pt is that the white line of Pt-PA is considerably more intense than that of the bulk. Moreover, we observed a positive shift (0.5 eV) of the

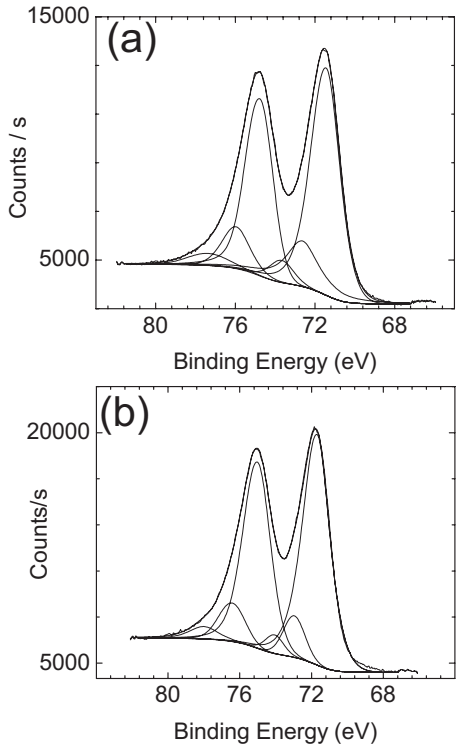

FIG. 4. Deconvoluted Pt 4f peaks of Pt-TA (a) and Pt-PA (b).

L_3-edge threshold energy (E_0) for Pt-PA relative to that of Pt foil. These observations indicate that the NPs have less d-electron counts than the bulk.[12] As is well known, the white line in XANES is mainly associated with the initial effect.[17] The XANES results thus provide a useful explanation to the XPS core-level BE shifts of Pt NPs presented in Fig. 2. The positive XPS BE shifts for Pt NPs should be largely associated with the initial state effect (charge depletion of Pt atoms), as evidenced by the fact that the BE shift of Pt-PA relative to the bulk (0.50 ± 0.10 eV) is in agreement with the XANES E_0 shift (0.5 ± 0.2 eV). Nevertheless, the contribution from the final state effect cannot be completely ruled out. It is also noted that the initial state effect unlikely results in the exactly same extent of BE shift for the deep 2p (XANES) and shallow 4f (XPS) core levels.

The observed enhancement of white line intensity of Pt-PA (d-charge depletion) and positive E_0 shift are in disagreement with the expectation based on the s-p-d hybridization theory presented above (i.e., Pt atoms in bare NPs gain d-electron). Cook *et al.*[8] reported a similar white line intensity increase for Pd NPs relative to the bulk. Such an increase in white line intensity was attributed to the partial surface oxidation effect of the NP surface, which was supported by Pd L_3-edge XANES simulations.[8] Based on this, we proposed that the observed increase in white line intensity for Pt-PA is similarly attributed to partial surface oxidation of Pt NPs (also see the deconvoluted XPS spectra presented next). Similar experimental evidence has been reported in the literature that oxide species are often present on the surface of Pt NP fuel cell catalysts.[2]

To analyze the surface oxidation behavior of the two weakly bound NPs, we next show the deconvoluted Pt 4f XPS spectra in Fig. 4. The peak-fitting analysis follows the method reported by Zhang *et al.*[21] After a Shirley background removal, the component peaks were separated using mixed Gaussian–Lorentzian functions. It is seen that for both Pt-PA and Pt-TA, there are three Pt species present. The first one (with lowest BE) can be attributed to zero-valent Pt. The other two peaks with higher BE are most likely oxide species, plausibly being PtO and PtOH species, which are commonly observed on Pt NP surfaces.[2] Our results are consistent with the Pt 4f XPS data reported by Zhang *et al.*, who observed two similar oxide peaks in the Pt NPs prepared on carbon nanotubes.

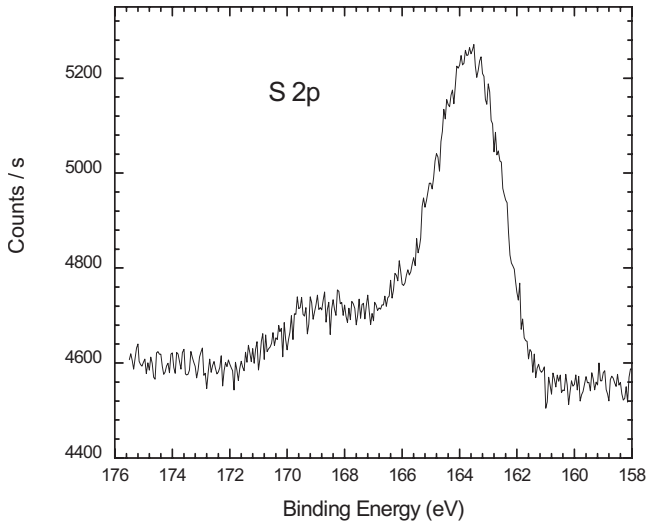

FIG. 5. S 2p XPS of Pt-SR.

Returning to the XPS Pt 4f data of Pt-PA and Pt-SR in Fig. 2, we now discuss the BE shift along with the linewidth broadening caused by the capping molecule effect (amine versus thiol) for the two same-sized NPs. Büttner *et al.*[22] studied the 4f and valence band results of Au NPs before and after thiol adsorption and similar positive BE shift was reported. This finding is consistent with our calculation results discussed later in Sec. III C. Thus the positive BE shift of Pt-SR relative to Pt-PA by 0.13 eV can be attributed to the surface effect, i.e., presence of Pt-SR species. This observation is comparable with the XPS data of Fu *et al.*[23] that a positive BE shift of 0.3 eV was found when thiols replaced amine capping molecules for 1.3 nm Pt NPs. However, our observation that Pt-SR shows a 4f linewidth broadening relative to that of Pt-PA, which was not observed in Büttner's work. Note that the NPs used in this work were prepared wet-chemically whereas in Büttner's work the NPs were prepared with a vacuum evaporation method.

To study the surface property of Pt-SR from sulfur perspective, we present the S 2p XPS spectrum of Pt-SR in Fig. 5. An intense peak at around 163.4 eV was observed. A weak and broad band at around 169 eV was also seen in the figure. Tu *et al.*[24] reported a sulfur 2p peak originating from an alkanethiol coating on Pt NPs. They showed that the S 2p peak of thiol-capped Pt NPs is located at 163.2 eV. This is a shift of 0.6 eV to lower BE with respect to that of the pure octadecanethiol molecules (163.8 eV).[24] The S 2p peak of our sample Pt-SR (note that our Pt-SR is capped with dodecylthiol) is located at 163.4 eV that corresponds to 0.4 eV of

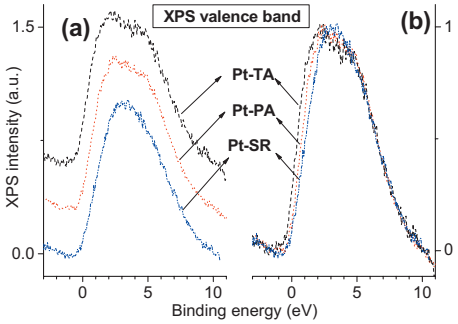

FIG. 6. XPS Pt 5d valence bands of three NPs.

shift to lower BE with respect to that of pure octadecanethiol.[24] Our finding of 163.4 eV for the S 2p peak seems to be in good agreement with the S 2p results of Tu *et al.*[24] and Fu *et al.*[23] The weak band at around 169 eV is most likely oxidized sulfur species,[25] which may be an indication of partial oxidation of the thiolate on the NP surface.

C. The valence band data and l-DOS calculation

Valence band spectra of the three samples are shown in Fig. 6. Quantitative valence band data are given in Table III. Relative to that of the bulk, the valence spectra of Pt-SR show the greatest shift of 5d centroid (0.42 eV), followed by Pt-PA (0.35 eV), and then Pt-TA (0.15 eV). In other words, the Pt 5d band centroids of the three NPs systematically move away from Fermi level relative to the bulk. Width of 5d band of the three NPs (5.35–5.90 eV) are all narrower than that of the bulk (6.30 eV). The 5d band width of Pt-SR is the narrowest (5.35 eV), followed by Pt-PA (5.50 eV) and it is widest for Pt-TA (5.90 eV) among the three NPs. Also the 5d bands of samples of Pt-TA and Pt-PA show developing of a second peak on the higher BE side separated by approximately 2 eV. This developing is more noticeable for Pt-TA.

To illustrate the origin of the observed valence band changes, a self-consistent real space Green's function approach implemented in *ab initio* FEFF8 program[10] was used to calculate the l-DOS using a representative Pt atomic site in bulk Pt and three model clusters, Pt_{55}, $Pt_{55}O_{24}$, and $Pt_{55}S_{24}$. The electronic configuration and charge transfer results are provided in Table IV. The calculated d-band results are presented in Fig. 7. It should be noted that our calculations are intended to qualitatively demonstrate the effects of nanosize (Pt_{55} versus bulk) and surface chemistry (Pt_{55} versus $Pt_{55}O_{24}$ and $Pt_{55}S_{24}$). Therefore, only a representative surface site (the vertex site marked by an arrow in Fig. 7) was chosen for such a demonstration. Calculation of the whole cluster can also be done by weight averaging the results of each representative site. Herein, we only intend to use one representative site to show the general trend of d-DOS change caused by the size and surface effect. The results in Table IV clearly support the s-p-d rehybridization model[9] we used to account for the Pt 4f BE shift. The bare cluster Pt_{55} shows a net charge increase of 0.395 e^- relative to the bulk, accompanied with a d-charge gain of 0.168 e^- (note: this is the result for only one atomic site, not for the whole cluster). In contrast, both $Pt_{55}O_{24}$ and $Pt_{55}S_{24}$ show charge depletion relative to the bulk. The $Pt_{55}O_{24}$ cluster shows a more significant decrease in electron counts relative to that of $Pt_{55}S_{24}$, presumably due to the greater electronegativity of oxygen than sulfur. It is also noticed that the $Pt_{55}O_{24}$ cluster only exhibits a very small amount of d-charge depletion (0.01 e^-) relative to the bulk. This seems somewhat inconsistent with the XANES results in Fig. 3 where a pronounced increase in the Pt L_3-edge white line is observed. However, it can be understandable if one considers that the bulk and $Pt_{55}O_{24}$ are different from the perspective of both the size and surface effects. The former effect normally leads to a gain of d-charge whereas the latter induces a d-charge depletion. Indeed, if one only considers the effect of surface chemistry by comparing the d-charge count of Pt_{55} with that of $Pt_{55}O_{24}$ (the nanosize effect is excluded), a fairly large amount of d-charge depletion (0.177 e^-) is found. Therefore, the unusually small change of d-charge count when going from $Pt_{55}O_{24}$ to the bulk can be accounted for by the interplay of

TABLE III. Pt 5d valence band data (Uncertainty: 0.20 eV) of three NPs and the bulk.

Sample	5d centroid (eV)	5d width (eV)
Pt-TA	3.25	5.90
Pt-PA	3.45	5.50
Pt-SR	3.52	5.35
bulk	3.10	6.30

TABLE IV. Results of calculated l-DOS of Pt model clusters.

Model	Electron configuration	Charge transfer (e^-)
$Pt_{55}S_{24}$	$s^{0.767}p^{0.816}d^{8.391}$	0.028
$Pt_{55}O_{24}$	$s^{0.754}p^{0.719}d^{8.454}$	0.073
Pt_{55}	$s^{0.870}p^{0.910}d^{8.631}$	−0.395
Bulk Pt	$s^{0.748}p^{0.789}d^{8.463}$	0

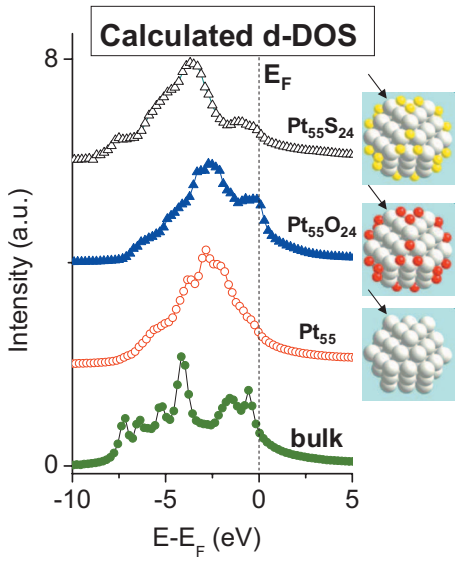

FIG. 7. Calculated d-DOS of one surface site (marked be an arrow) of $Pt_{55}S_{24}$, $Pt_{55}O_{24}$, Pt_{55}, and that of the bulk.

the size and surface effect. It is expected that at other surface sites (e.g., terrace site) where the coordination number is higher than that shown in Fig. 7, the d-charge depletion of Pt atoms should be more pronounced than the result in Table IV, since the d-charge-gaining size effect is less significant for a higher coordination number. Consequently, the overall d-charge depletion for the $Pt_{55}O_{24}$ cluster (i.e., the averaged result of all the atomic sites) is expected to be more pronounced than the data given in Table IV.

In Fig. 7, the nanosize effect is clearly illustrated by a significant d-band narrowing of the three clusters relative to that of the bulk. The surface effect can be seen by comparing d-bands of the three clusters with varied surface chemistry. The presence of thiolates and oxides both result in a new feature near the Fermi level. It is evident that the presence of thiolates (S atoms) causes a considerable positive shift of BE. In contrast, the effect of surface oxides cause no noticeable change of BE when going from Pt_{55} to $Pt_{55}O_{24}$. It is also observed in Fig. 7 that the surface effect (sulfur or oxygen) causes almost no change of 5d band linewidth. Based on these calculation results, we now discuss the experimental valence band results in Fig. 6. The observed narrowing of Pt 5d bands when going from bulk to Pt-TA and then to Pt-PA should be mainly caused by the nanosize effect. However, the d-band narrowing (0.15 eV) after thiol adsorption (Pt-PA → Pt-SR) cannot be interpreted using the standard thiolate-capping model shown in Fig. 7. It implies that some different Pt-thiolate surface structure may be present. The observed shift of d-band centroid for the two weakly bound Pt NPs is plausibly caused by the size effect, that is, a shift associated with the d-band narrowing rather than the surface effect (oxide). In addition, the d-band shift when going from Pt-PA to Pt-SR should be largely related to the surface effect, as the two NPs have identical size. The reason that the calculated d-DOS surface states (oxide and thiolate) near the Fermi level was not resolved in the experimental valence band spectra is probably because concentrations of the surface oxides and thiolates in the NPs are not high enough. Another possible reason could be due to the limited detection sensitivity of XPS valence band spectra, which can be enhanced in future works by ultraviolet photoelectron spectroscopy (UPS) experiments.

D. Toward tuning the electronic properties of Pt NPs

Finally, we correlate the surface and electronic properties of Pt NPs discussed above with the possibility of systematically tuning their electronic properties. The above x-ray data indicate that the Pt NPs tend to lose d-electrons counts due to the presence of surface oxide (or thiolate). In order to systematically tune the electronic properties of these NPs, a challenge that remains is how to increase the d-electron (5d) density in Pt NPs. Recently, we have reported that for Pd NPs, although the surface effect (oxide or thiolate) resulted in a d-electron depletion in Pd NPs, an increase in d-electron counts can be achieved by forming PdAg bimetallic NPs.[8] Based on this finding, we prepared a sample of PtAu NPs (Pt:Au=1:1) using the same method for the preparation of Pt-PA in order to explore the possibility of increasing the d-electron density of Pt in the NPs. In Fig. 8, we present Pt L_3-edge XANES data of PA-protected Pt and PtAu NPs. It is evident that introduction of Au causes a noticeable decrease in Pt L_3-edge white line, implying an increase in d-electron counts.[9] The results in Fig. 8 thus demonstrate that formation of PtAu alloying interaction in Pt NPs presents an efficient way to increase the d-electron count of Pt NPs. It should be noted that the increase in Pt d-charge counts caused by the introduction of Au atoms does not conflict with the electronegativity data (Au > Pt). For instance, it was found that electronegative Au atoms lost d-electron but gained non-d-electron when forming an alloy with less electropositive Ag atoms, which resulted in a net increase in the total electron density of Au atoms.[26]

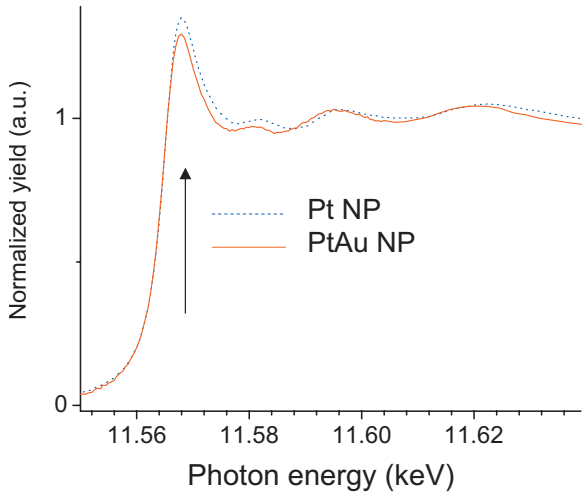

FIG. 8. Pt L_3-edge XANES of PA-protected Pt and PtAu NPs prepared under identical conditions.

IV. CONCLUSION

We have presented a detailed study on the surface structure and electronic properties of molecularly capped Pt NPs using XPS, XAS, and l-DOS calculations. The effects of nanosize and surface structure of the NPs on the core-level and valence band XPS were revealed. The mechanism of the size and surface effects on the electronic properties of Pt NPs was illustrated by correlating the XPS data with XAS and theoretical d-DOS results. Finally, the implication on systematically tuning the d-electron behavior of Pt NPs by manipulating the surface, size, and alloying effects was discussed.

ACKNOWLEDGMENTS

The research is financially supported by Dalhousie University and NSERC Canada. The authors acknowledge financial support from NSERC, the Killam Trusts, Canada Foundation for Innovation (CFI), the Atlantic Innovation Fund, and other partners that fund the Facilities for Characterization of Materials managed by the Institute of Materials for Research (IRM). The Canadian light source (CLS) is supported by NSERC, CIHR, NRC, and the University of Saskatchewan. The CLS staff scientist Dr. Ning Chen is acknowledged for the synchrotron technical support.

[1] G. A. Somorjai, R. L. York, D. Butcher, and J. Y. Park, Phys. Chem. Chem. Phys. **9**, 3500 (2007); S. H. Joo, S. J. Choi, I. Oh, J. Kwak, Z. Liu, O. Terasaki, and R. Ryoo, Nature (London) **412**, 169 (2001).
[2] J. Zhang, K. Sasaki, E. Sutter, and R. R. Adzic, Science **315**, 220 (2007).
[3] B. L. Cushing, V. L. Kolesnichenko, and C. J. O'Connor, Chem. Rev. **104**, 3893 (2004); J. A. Dahl, B. L. S. Maddux, and J. E. Hutchison, *ibid.* **107**, 2228 (2007); R. Ferrando, J. Jellinek, and R. L. Johnston, *ibid.* **108**, 845 (2008).
[4] M. C. Daniel and D. Astruc, Chem. Rev. **104**, 293 (2004).
[5] C. J. Murphy, T. K. San, A. M. Gole, C. J. Orendorff, J. X. Gao, L. Gou, S. E. Hunyadi, and T. Li, J. Phys. Chem. B **109**, 13857 (2005); L. F. Gou and C. J. Murphy, Chem. Mater. **17**, 3668 (2005).
[6] S. Krüger, S. Vent, F. Nortemann, M. Staufer, and N. Rosch, J. Chem. Phys. **115**, 2082 (2001); A. L. Ankudinov, J. J. Rehr, J. J. Low, and S. R. Bare, *ibid.* **116**, 1911 (2002).
[7] M. Brust, M. Walker, D. Bethell, D. J. Schiffrin, and R. Whyman, J. Chem. Soc., Chem. Commun. **1994**, 801.
[8] S. C. Cook, J. D. Padmos, and P. Zhang, J. Chem. Phys. **128**, 154705 (2008).
[9] F. Liu, D. Wechsler, and P. Zhang, Chem. Phys. Lett. **461**, 254 (2008).
[10] A. L. Ankudinov, B. Ravel, J. J. Rehr, and S. D. Conradson, Phys. Rev. B **58**, 7565 (1998).
[11] P. B. Murphy, F. Liu, S. C. Cook, N. Jahan, D. G. Marangoni, T. B. Grindley, and P. Zhang, Can. J. Chem. **87**, 1641 (2009).
[12] P. Zhang and T. K. Sham, Phys. Rev. Lett. **90**, 245502 (2003).
[13] S. Doniach and M. Sunjic, J. Phys. C **3**, 285 (1970).
[14] G. K. Wertheim, Z. Phys. D: At., Mol. Clusters **12**, 319 (1989).
[15] M. G. Mason, Phys. Rev. B **27**, 748 (1983).
[16] G. K. Wertheim, S. B. Dicenzo, and S. E. Youngquist, Phys. Rev. Lett. **51**, 2310 (1983).
[17] M. Cini, M. Decrescenzi, F. Patella, N. Motta, M. Sastry, F. Rochet, R. Pasquali, A. Balzarotti, and C. Verdozzi, Phys. Rev. B **41**, 5685 (1990).
[18] J. H. Sinfelt and G. D. Meitzner, Acc. Chem. Res. **26**, 1 (1993).
[19] M. G. Mason, L. J. Gerenser, and S. T. Lee, Phys. Rev. Lett. **39**, 288 (1977).
[20] L. F. Mattheiss and R. E. Dietz, Phys. Rev. B **22**, 1663 (1980).
[21] G. X. Zhang, D. Q. Yang, and E. Sacher, J. Phys. Chem. C **111**, 565 (2007).
[22] M. Büttner, H. Kroger, I. Gerhards, D. Mathys, and P. Oelhafen, Thin Solid Films **495**, 180 (2006).
[23] X. Y. Fu, Y. Wang, N. Z. Wu, L. L. Gui, and Y. Q. Tang, J. Colloid Interface Sci. **243**, 326 (2001).
[24] W. X. Tu, K. Takai, K. Fukui, A. Miyazaki, and T. Enoki, J. Phys. Chem. B **107**, 10134 (2003).
[25] J. A. Rodriguez and J. Hrbek, Acc. Chem. Res. **32**, 719 (1999).
[26] C. C. Tyson, A. Bzowski, P. Kristof, M. Kuhn, R. Sammynaiken, and T. K. Sham, Phys. Rev. B **45**, 8924 (1992).